ChemComm

$[Cp^*RuPb_{11}]^{3-}$ and $[Cu@Cp^*RuPb_{11}]^{2-}$: Centered and Non-Centered Transition-Metal Substituted Zintl Icosahedra.

Journal:	*ChemComm*
Manuscript ID	CC-COM-05-2020-003656.R2
Article Type:	Communication

COMMUNICATION

$[Cp^*RuPb_{11}]^{3-}$ and $[Cu@Cp^*RuPb_{11}]^{2-}$: Centered and Non-Centered Transition-Metal Substituted Zintl Icosahedra.

Received 00th January 20xx,
Accepted 00th January 20xx

DOI: 10.1039/x0xx00000x

Ai-Min Li,[a] Yi Wang,[a] Peter Zavalij,[a] Fu Chen,[a] Alvaro Muñoz-Castro,[b] and Bryan W. Eichhorn*[,a]

Cluster anions $[Cp^*RuPb_{11}]^{3-}$ (1) and $[Cu@Cp^*RuPb_{11}]^{2-}$ (2) represent the first vertex-substituted Zintl icosahedra and 1 is the first non-centered Zintl icosahedron isolated in the condensed phase. Complexes 1 and 2 are both 12-vertex, 26-electron *closo*-clusters with C_{5v} point symmetry and are static on the ^{207}Pb NMR time scale in solution.

Homoleptic and mixed-atom main-group icosahedra are emerging as a diverse class of highly symmetrical clusters that are reminiscent of the fullerenes.[1] In contrast to transition metal clusters, these Zintl phase species usually contain no supporting organic ligands, often possess rigorous I_h point symmetry and unusual electronic structures. Unlike the borane and transition metal icosahedra, such as $[B_{12}H_{12}]^{2-}$,[2] $C_2B_{10}H_{12}$,[3] $[3,3'\text{-}M(1,2\text{-}C_2B_9H_{11})_2]^-$ (M = Fe, Co, Ni) [4] and the hetero-nickel clusters, $[Ni_{10}(EMe)_2(CO)_{18}]^{2-}$ (E = P, As, Sb, Bi),[5] and $[Ni_8Te_4(CO)_{12}]^{2-}$,[6] the isolated examples of Zintl ion based icosahedra invariably contain endohedral metal atoms.[7] The homoleptic $[M@Pb_{12}]^{n-}$ clusters contain a range of endohedral metal atoms (M = Ni, Pd, Pt, Co, Rh, Ir, Au; n = 2, 3) [7a-7e] as do the mixed-atom complexes, such as the $[Tl@Tl_4Pb_8]^{4-}$ ion [8] and the *closo*-$[Pd@Pd_2Pb_{10}Bi_6]^{4-}$ polyhedron.[9] The $[Tl@Tl_{12}]^{11-}$ cluster [10] found in the $Na_3K_8Tl_{13}$ Zintl phase also confirms the tendency of embedding endohedral atoms in bare icosahedra. The ubiquitous occurrence of endohedral atoms suggest that their presence is necessary to either template or stabilize the structures through radial bonding. The large ^1J-coupling between the NMR spin-active endohedrals and the icosahedral vertices (e.g. $^1J_{^{207}Pb\text{-}^{195}Pt}$ = 3440 Hz for $[Pt@Pb_{12}]^{2-}$) are consistent with this hypothesis.[7c]

The presence of NMR spin-active nuclei (e.g. ^{119}Sn and ^{207}Pb; I = 1/2) in the $[M@Pb_{12}]^{n-}$ framework structures provides a powerful probe of bonding and fluxional properties. For example, the nine Sn atoms of $[Pt@Sn_9Pt(PPh_3)]^{2-}$,[11] are in fast exchange on the NMR time scale whereas the two Pt atoms are not. In contrast, the $[E_9M(CO)_3]^{4-}$ complexes where E = Sn, Pb; M = Cr, Mo, W, are static on the NMR time scale with no observable exchange of vertex atoms.[12]

We report here the synthesis and characterization of the $[Cp^*RuPb_{11}]^{3-}$ icosahedral cluster, (**1**) and the endohedral derivative $[Cu@Cp^*RuPb_{11}]^{2-}$, (**2**). Cluster **1** is the first ML_n vertex-substituted icosahedron and the first endohedral-free icosahedron in this class of Zintl clusters. ^{207}Pb NMR studies show that insertion of the Cp*Ru vertex into the framework renders both **1** and **2** static on the NMR time scale. ^{63}Cu NMR studies on **2** show that the static structure and its inherent asymmetry fail to eliminate the quadrupolar effects observed in other symmetric endohedral Cu^+ complexes. The Cp*Ru vertex substitution also causes static distortions in the structures of both **1** and **2** that are not present in the homoleptic icosahedra. The absence of an endohedral metal atom in **1** suggests that other endohederal-free icosahedra, such as those observed in the gas phase, may be accessible in the condensed phase.

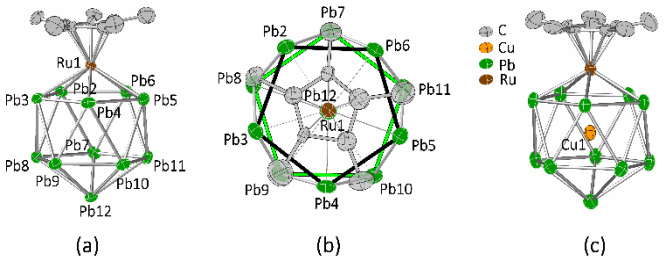

Fig. 1 ORTEP drawings of the $[Cp^*RuPb_{11}]^{3-}$ ion, **1**, showing (a) a side view and (b) a top view down the Ru1–Pb12 axis. For clarity, the two different Pb_5 pentagonal planes normal to the Ru1–Pb12 axis are shown in different colors (black and light green). (c) ORTEP drawing of the $[Cu@Cp^*RuPb_{11}]^{2-}$ ion, **2**. Thermal ellipsoids were drawn at the 50% probability level.

[a] *Department of Chemistry and Biochemistry, University of Maryland, College Park, MD 20742, USA*
[b] *Laboratorio de Química Inorgánica y Materiales Moleculares, Facultad de Ingeniería, Universidad Autonoma de Chile, Llano Subercaseaux 2801, San Miguel, Santiago, Chile*

Electronic Supplementary Information (ESI) available: X-ray crystallographic in CIF format, full experimental, LDI-TOF mass spectra, computational details and the supporting figures are available. CCDC 1999074–1999075. For ESI and crystallographic data in CIF or other electronic format see DOI: 10.1039/x0xx00000x

The {[K(18-crown-6)]$_2$[K(en)$_2$(18-crown-6)]}(**1**) salt is monoclinic, space group *C2/c* and contains non-interacting [Cp*RuPb$_{11}$]$^{3-}$ icosahedra (Fig. 1a) with two [K(18-crown-6)]$^+$ and one [K(en)$_2$(18-crown-6)]$^+$ cations per anion (Fig. S1a). The two [K(18-crown-6)]$^+$ cations and the [K(en)$_2$(18-crown-6)]$^+$ cation show some disorder, which was successfully modeled. Both of the [K(18-crown-6)]$^+$ cations are coordinated to the cluster through K$^+$···Pb interactions (3.719(3) Å, ave). A summary of the crystallographic data is given in Table S1 and the selected bond distances are given in Tables S2 of the Supporting Information. The [Cp*RuPb$_{11}$]$^{3-}$ anion contains eleven Pb atoms and one Ru atom that define the vertices of the icosahedral cage (Fig. 1a). The η^5-Cp* ligand symmetrically caps the Ru atom and is in a staggered configuration with respect to the top Pb$_5$ ring (Pb2–Pb6), giving overall C_{5v} molecular symmetry (Fig. 1b). Using a Wade-Mingos electron accounting analysis,[13] each Pb atom contributes two electrons to cluster bonding, the Cp*Ru moiety contributes one electron, and the -3 charge provides three electrons to give 26 cluster bonding electrons [(11 x 2) + 1 + 3 = 26] and a 2n+2 *closo* architecture where n is the number of deltahedral vertices. As such, the [Cp*RuPb$_{11}$]$^{3-}$ cluster anion possesses a 12-vertex, 26-electron *closo* structure and is isostructural and isoelectronic to the [Cp*RuC$_2$B$_9$H$_{11}$] metallocarborane.[14]

The icosahedral framework of **1** is distorted relative to known endohedral [M@Pb$_{12}$]$^{n-}$ clusters containing homoleptic vertices (M = Ni, Pd, Pt, Co, Rh, Ir, Au; n = 2, 3).[7a-7e] The major impact on structure results from the five short Ru–Pb contacts (2.9304(12) Å, ave.) relative to the average of the 25 Pb–Pb contacts (3.166(9) Å, ave.). As a result, the Pb–Pb contacts within the top square plane (Pb2 through Pb6) are statistically shorter (3.023(8) Å, ave.) relative to the Pb–Pb contacts in the remainder of the structure. The ten Pb–Pb contacts between the top and bottom pentagonal planes are the longest at 3.235(9) Å, ave., whereas the remainder average 3.113(9) Å. These asymmetries result in three groupings of Pb–Pb contacts: short contacts within the top pentagonal plane, long contacts between pentagonal planes and "normal" contacts within the bottom pentagonal plane (Pb7 through Pb11) and to the Pb12 vertex. For reference, the Pb–Pb contacts in the [M@Pb$_{12}$]$^{n-}$ clusters have averages that span the range from 3.078Å (Ni)[7a] to 3.216 Å (Pt).[7c] In addition, the distortions observed in **1** are quite different from those observed in the related [E$_9$]$^{4-}$ ions (E = Sn, Pb) and their metallated [*closo*-E$_9$M(CO)$_3$]$_{4-}$ derivatives (M = Cr, Mo, W; E = Sn, Pb) [12] where the interatom contacts within the bottom planes are elongated.

As expected, the electron deficient Ru–Pb contacts in **1** are longer than 2c-2e Ru–Pb bonds reported in the literature, which span the range from 2.667(5) Å to 2.802(6) Å.[15] The Ru–Pb bonds in **1** are more akin to the Mo–Pb bonds (3.001(6)–3.093(7) Å) found in the planar *cyclo*-[{(OC)$_3$Mo}Pb$_5${Mo(CO)$_3$}]$^{4-}$ ion.[16] The Ru–C distances to the Cp* ligand average 2.201(14) Å are significantly longer than those in the related Cp*Ru-metallaborane complexes (1.819 Å),[17] but are comparable to other Cp*Ru-compounds that are less electron deficient (2.15 Å ~ 2.25 Å).[18]

The {[K(18-crown-6)]$_2$(tol)$_2$}(**2**) salt is triclinic, space group *P-1* (No. 2), and contains two toluene solvate molecules in the crystal lattice. A summary of the crystallographic data is given in Table S1. Selected bond distances and angles for the clusters are given in Tables S3. Both of the [K(18-crown-6)]$^+$ cations are coordinated to the cluster through K$^+$···Pb interactions (3.693(6) Å, ave), with one of the [K(18-crown-6)]$^+$ cations being disordered in two different orientations. The structure of the [Cu@Cp*RuPb$_{11}$]$^{2-}$ ion, **2**, is shown in Fig. 1c. The formal insertion of the Cu$^+$ ion into the [Cp*RuPb$_{11}$]$^{3-}$ cluster results in an overall -2 charge for 2 but does not alter the total electron count due to the d^{10} configuration of the cuprous ion.[19] As such, **2** is also a C_{5v} 12-vertex, 26-electron *closo* cluster and is isostructural to **1**. The average metric parameters of **2** are statistically equivalent to those of **1** except for a slight contraction within the top pentagonal plane. The groupings of bond distances persist in 2 with short contacts within the top pentagonal plane (3.068(18) Å, ave.), long contacts between pentagonal planes (3.267(7) Å, ave.) and "normal" contacts within the bottom pentagonal plane and to the Pb12 vertex (3.182(5) Å, ave.). The five Ru–Pb contacts and the 11 Cu–Pb average 2.945(7) Å and 3.011(11) Å, respectively. The Cu$^+$ is symmetrically centered within the icosahedral structure with the exception of the shorter Cu–Ru contact (2.843(1) Å) relative to the longer Cu–Pb12 contact (3.075(1) Å). The Cu–Pb contacts in **2** are significantly longer than the 2.700(7) Å contacts found in the related [Cu@Pb$_9$]$^{3-}$ ion.[20]

The ^{207}Pb NMR spectrum of the [Cp*RuPb$_{11}$]$^{3-}$ cluster, **1**, (Fig. S10) shows three ^{207}Pb resonances at 315, -88 and -365 ppm, with the expected relative intensity ratio of 5:5:1. These data are consistent with expectations based on the solid state structure and show that the cluster is static on the ^{207}Pb NMR time scale, as described below. Based on the integrated peak intensities, the three resonances can be assigned to the two pentagon rings and the unique vertex Pb atom, respectively. The 315 and -88 ppm peaks each contains satellite doublets ($^1J_{207Pb\text{-}207Pb}$ = 4198 Hz) with relative intensities of 1.0 : 3.8 : 1.0 (averaged over several experiments). The satellites arise from $^1J_{207Pb\text{-}207Pb}$ mutual coupling between the chemically distinct Pb atoms of adjacent Pb$_5$ pentagonal rings. In the solid-state structure, the Pb atoms in each pentagonal ring are bound to two chemically equivalent Pb atoms within their own ring and two chemically inequivalent Pb atoms in the adjacent ring. Only coupling to the inequivalent ^{207}Pb atoms is observed experimentally and gives rise to the satellite patterns on the 315 and -88 ppm peaks. Using a statistical analysis of isotopic coupling between chemically inequivalent ^{207}Pb atoms (^{207}Pb, I = ½; abund = 22.1%), one predicts a 1.00 : 3.66 : 1.00 intensity ratio for the central resonance and its satellites, which is similar to the experimentally observed ratio. The 4198 Hz $^1J_{207Pb\text{-}207Pb}$ interplanar coupling in **1** is similar to that observed in the related *closo*-[1-Mo(CO)$_3$(η^4-Pb$_9$)]$^{4-}$ anion (4500 Hz).[12e] The ^{207}Pb NMR resonance at -365 ppm is a second order resonance arising from the apical Pb12 atom in **1**. The pattern shows a central peak at -365 ppm with 4 other primary lines at non-interval spacings (Fig. S10).

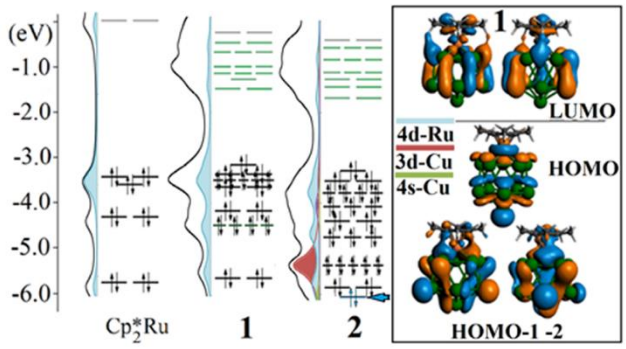

Fig. 2 Electronic structure for Cp^*_2Ru, **1**, and **2**, and frontier orbitals for **1**. Total density of states (black) and PDOS for 4d-Ru, 3d-Cu, and 4s-Cu. Green levels denote the main Pb_{11} character.

Spectra collected from different crystalline samples at three different magnetic field strengths (Fig. S12) give the same multiplet pattern with the same peak separation in Hz, indicating that the multiplet arises from second order coupling associated with the Pb12 atom.

The insertion of Cu^{+1} ion into the $[Cp^*RuPb_{11}]^{3-}$ cluster gives the $[Cu@Cp^*RuPb_{11}]^{2-}$ ion, **2**, which shows significant upfield shifts of the Pb signals relative to the parent ion **1** (Fig. S11, left). Cluster **2** remains static on the NMR time scale and shows two equal intensity resonances associated with the top and bottom pentagonal rings. The signals appear at -430 ppm and -623 ppm, which are more than 500 ppm upfield from the corresponding resonances of **1**. The ~4900 Hz $^1J_{207Pb-207Pb}$ coupling between the two rings is similar to that of **1** but is poorly resolved due to the lower signal-to-noise ratio of the spectrum. The resonance for the Pb12 atom of **2** was not located. The ^{63}Cu NMR signal for 2 appears as a broad resonance centered at 885 ppm, with a line width of 9015 Hz (Fig. S11, right). The peak is downfield by 1215 ppm compared to the related $[Cu@Pb_9]^{3-}$ and $[Cu@Sn_9]^{3-}$ ions[20] and is significantly broadened due to the quadrupolar nature of the ^{63}Cu nucleus (^{63}Cu, I = 3/2; abund = 69.2%). In the $[Cu@E_9]^{3-}$ complexes, the quadrupolar broadening is eliminated due to the symmetrical environment of the endohedral Cu^{+1} ion provided by the fluxional behavior of the Pb_9 cage and the ^{63}Cu NMR spectra are sharp with well-defined coupling. The inherent asymmetry of **2** precludes the elimination of quadrupolar broadening. The data show that clusters **1** and **2** are static on the ^{207}Pb NMR time scale. The three distinct resonances observed for **1** show that there is no exchange between the pentagonal rings or the apical Pb12 atom. In addition, the integrated satellite intensities on the signals for the pentagonal rings show that each Pb atom is only in contact with two Pb atoms on a neighboring pentagonal ring, which shows that Pb exchange within the pentagonal rings is also slow on the ^{207}Pb NMR time scale.

The electrospray-ionization time-of-flight (ESI-TOF) mass spectra for $[K(18\text{-crown-6})]_2[K(18\text{-crown-6})(en)_2]$(**1**) and $\{[K(18\text{-crown-6})]_2(tol)_2\}$(**2**) salts dissolved in CH_3CN are shown in Fig. S3–S7. Intense peaks are observed for the oxidized parent ions of **1** and **2** along with the expected K^+ and $(K\text{-crown})^+$ ion pairs of the molecular ions. Stable gas phase degradation products are also observed in the spectra, including $[Cp^*RuPb_6]^{1-}$, $[Cp^*RuPb_{10}]^{1-}$, $[Cu@Pb_{10}]^{1-}$ and $[Ru@Pb_{11}]^{1-}$ (Fig. S6–S7).

The electronic structure of $[Cp^*RuPb_{11}]^{3-}$ and $[Cu@Cp^*RuPb_{11}]^{2-}$ were investigated via density functional theory calculations, which revealed a sizable HOMO-LUMO gaps of 1.638 eV and 1.611 eV, respectively, indicating stability of the clusters similar to other bare and ligand-protected clusters.[21]

For comparison, the HOMO-LUMO gap for Cp^*_2Ru is 3.412 eV (Fig. S15). This difference originates from the frontier orbitals of **1** and **2**, being largely composed by the *nido*-Pb_{11}^{4-} fragment high-lying orbitals (green lines in Fig. 2). These frontier fragment orbitals have a significant overlap with the Cp^*Ru^+ fragment. For Cp^*_2Ru, the HOMO and LUMO are of mainly *d*-metal and ligand character, respectively, as usual for metallocenes.[22]

Projected density of states (PDOS) is given for each species in order to account for the contribution from 4d-Ru, 3d-Cu, and, 4s-Cu shells (Fig. 2), where the 3d-Cu shell remains as a non-bonding shell in the electronic structure for **2**, and thus not contributing to the stabilization of the $Pb_{11}Ru$ cage. For all the systems, 4d-Ru orbitals contribute mainly at the frontier orbitals, accounting for the ruthenocene resemblance of **1** and **2**.

For **1** and **2**, the main interactions involve the valence-electron system containing the tangential orbitals of the parent *nido*-Pb_{11}^{4-} cage and the $d_{x2-y2}/d_{xy}/d_{z2}$-Ru (HOMO, HOMO-1, HOMO-2) orbitals, resulting in a bonding scheme related to Cp^*_2Ru. Slight differences are found between **1** and **2**, where the main characteristic of the later is the appearance of a bonding orbital involving the 4s-Cu levels and a totally symmetric tangential shell composed by 3p-Pb and $4d_{z2}$-Ru atomic orbitals (blue arrow bottom in Fig. 2, and supporting information), as responsible for the bonding stabilization of the endohedral copper atom, in addition to the non-bonding 3d-Cu shells. Moreover, the localized molecular orbital (LMO) analysis reveals the resemblance between **1** and **2** as 26 cluster bonding electrons species, where 3d-Cu levels appear as five lone-pairs (1c-2e) not contributing to the cage bonding. The *closo*-characteristics of their icosahedral cage, suggest an aromatic behavior reminiscent to I_h-Pb_{12}^{2-} and related group 9 and 10 endohedrals.[7a-7c, 23] The calculated NICS value at the center of the cage **1** shows a shielding of -24.0 ppm, similar in magnitude to the obtained for *closo*-Pb_{12}^{2-} (-28.6 ppm),[24] supporting the presence of a spherical aromatic character which is also extensible for **2**.

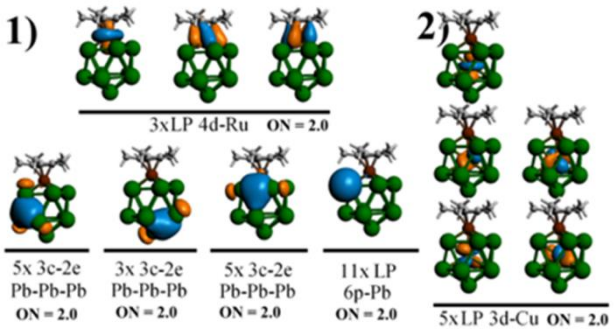

Fig. 3 Localized Molecular Orbitals (LMO) for **1** and **2**, Note the Lone-Pair (LP) character of 3d-Cu orbitals in **2** (1c-2e 3d-Cu). Occupation numbers (ON) are given.

Moreover, the Cp*Ru-cage interactions within the related Cp^*_2Ru, $[Cp^*RuC_2B_9H_{11}]^{1-}$, and the new structures **1** and **2**, was evaluated via calculations. The analysis shows an increase in interaction along the series from -208.5 < -299.4 < -390.6 < -327.9 kcal·mol^{-1}, respectively. This difference is given by the enhanced electrostatic character provided by the formal $[C_2B_9H_{11}]^{2-}$, $[Pb_{11}]^{4-}$, and $[Cu@Pb_{11}]^{3-}$, resulting in a more favorable Cp*Ru-cage interaction in the new species.

In the present work, we describe the synthesis and characterization of two new vertex-substituted icosahedral clusters $[Cp^*RuPb_{11}]^{3-}$ (**1**) and $[Cu@Cp^*RuPb_{11}]^2$ (**2**). These two clusters are the first example of vertex-substituted Zintl icosahedra and ion **1** is the first non-centered Zintl icosahedron isolated in the condensed phase. The $RuPb_{11}$ icosahedral frameworks of both **1** and **2** are static on the ^{207}Pb NMR time scale at room temperature showing three distinct, mutually-coupled ^{207}Pb NMR resonances with the expected 5:5:1 intensity ratios.

This work was supported by the Office of Naval Research through MURI - N00014-15-1-2681 and FONDECYT 1180683.

Conflicts of interest

There are no conflicts to declare.

Notes and references

1 (a) R. J. N. Lichtenberger, B. Weinert and S. Dehnen, *Chem. Rev.*, 2019, **119**, 8506; (b) S. Scharfe, F. Kraus, S. Stegmaier, A. Schier and T. F. Fässler, *Angew. Chem. Int. Ed*., 2011, **50**, 3630; *Angew. Chem*., 2011, **123**, 3712; (c) M. J. Moses, J. C. Fettinger and B. W. Eichhorn, *Science*, 2003, **300**, 778; (d) S. Stegmaier, and T. F. Fässler, *J. Am. Chem. Soc.*, 2011, **133**, 19758.

2 (a) A. R. Pitochelli and F. M. Hawthorne, *J. Am. Chem. Soc.,* 1960, **82**, 3228; (b) I. B. Sivaev, V. I. Bregadze and S. Sjöberg, *Collect. Czech. Chem. Commun.,* 2002, **67**, 679.

3 (a) V. I. Bregadze, *Chem. Rev.,* 1992, **92**, 209; (b) R. N. Grimes, *Structure and Bonding*. In *Carboranes*; Academic Press: Cambridge, MA, USA, 2016, 7.

4 (a) I. B. Sivaev, and V. I. Bregadze, *J. Organomet. Chem.,* 2000, **614**, 27; (b) I. B. Sivaev and V. I. Bregadze, *Collect. Czech. Chem. Commun.,* 1999, **64**, 783; (c) M. F. Hawthorne, D. C. Young, T. D. Andrews, D. V. Howe, R. L. Pilling, A. D. Pitts, M. Reintjes, L. F. Warren Jr, and P. A. Wegner, *J. Am. Chem. Soc.,* 1968, **90**, 879.

5 (a) D. F. Rieck, R. A. Montag, T. S. McKechnie and L. F. Dahl. *J. Am. Chem. Soc.,* 1986, **108**, 1330; (b) D. F. Rieck, J. A. Gavney Jr, R. L. Norman, R. K. Hayashi and L. F. Dahl. *J. Am. Chem. Soc.,* 1992, **114**, 10369; (c) P. D. Mlynek, and L. F. Dahl, *Organometallics,* 1997, **16**, 1655.

6 A. J. Kahaian, J. B. Thoden, and L. F. Dahl, *J. Chem. Soc., Chem. Commun.,* 1992, **4**, 353.

7 (a) E. N. Esenturk, J. Fettinger, and B. Eichhorn, *J. Am. Chem. Soc.,* 2006, **128**, 9178; (b) A. M. Li, Y. Wang, O. Downing, F. Chen, P. Y. Zavalij, A. Muñoz-Castro, and B. Eichhorn, *Chem. Eur. J.,* 2020*,* **26**, 5824*;* (c) E. N. Esenturk, J. Fettinger, Y. F. Lam, and B. Eichhorn, *Angew. Chem. Int. Ed*., 2004, **43**, 2132; *Angew.Chem.* 2004, **116**, 2184; (d) L. J. Li, F. X. Pan, F. Y. Li, Z. F. Chen, and Z. M. Sun, *Inorg. Chem. Front.,* 2017, **4**, 1393; (e) Y. Wang, L. L. Wang, H. P. Ruan, B. L. Luo, R. L. Sang, and L. Xu, *Chinese J. Struct. Chem.* 2015, **34**, 1253; (f) J. Q. Wang, S. Stegmaier, B. Wahl, T. F. Fässler, *Chem. Eur. J.,* 2010, **16**, 1793; (g) C. Liu, L.-J. Li, I. A. Popov, R. J. Wilson, C.-Q. Xu, J. Li, A. I. Boldyrev, and Z.-M. Sun, *Chin. J. Chem.* 2018, **36**, 1165; (h) C. Liu, N. V. Tkachenko, I. A. Popov, N. Fedik, X. Min, C.-Q. Xu, J. Li, J. E. McGrady, A. I. Boldyrev, and Z.-M. Sun, *Angew. Chem. Int. Ed.,* 2019, **58**,8367; *Angew. Chem.* 2019, **131**, 8455.

8 N. Lichtenberger, Y. J. Franzke, W. Massa, F. Weigend and S. Dehnen, *Chem. Eur. J.,* 2018, **24**, 12022.

9 R. Ababei, W. Massa, K. Harms, X. Xie, F. Weigend and S. Dehnen, *Angew. Chem. Int. Ed.* 2013, **52**, 13544; *Angew. Chem.* 2013, **125**, 13786.

10 Z. C. Dong and J. D. Corbett, *J. Am. Chem. Soc.,* 1995, **117**, 6447.

11 B. Kesanli, J. Fettinger, D. R. Gardner and B. Eichhorn, *J. Am. Chem. Soc.,* 2002, **124**, 4779.

12 (a) J. Campbell, H. P. Mercier, H. Franke, D. P. Santry, D. A. Dixon and G. J. Schrobilgen, *Inorg. Chem.,* 2002, **41**, 86; (b) B. Kesanli, J. Fettinger and B. Eichhorn, *Chem. Eur. J.,* 2001, **7**, 5277; (c) B. W. Eichhorn, R. C. Haushalter and W. T. Pennington, *J. Am. Chem. Soc.,* 1988, **110**, 8704; (d) B. W. Eichhorn and R. C. Haushalter, *J. Chem. Soc., Chem. Commun.,* 1990, **13**, 937; (e) W. L. Wilson, R. W. Rudolph, L. L. Lohr, R. C. Taylor and P. Pyykkö, *Inorg. Chem.,* 1986, **25**, 1535.

13 (a) K. Wade, *Adv. Inorg. Chem. Radiochem*., 1976, **18**, 1; (b) D. M. P. Mingos, *Nature Phys. Sci.,* 1972, **236**, 99; (c) J. W. Lauher, *J. Am. Chem. Soc.* 1978, **100**, 5305.

14 A. R. Kudinov, D. S. Perekalin, S. S. Rynin, K. A. Lyssenko, G. V. Grintselev-Knyazev and P. V. Petrovskii, *Angew. Chem. Int. Ed.,* 2002, **41**, 4112; *Angew. Chem.,* 2002, **114**, 4286.

15 (a) R. D. Adams, B. Captain and W. Fu, *J. Organomet. Chem.,* 2003, **671**, 158; (b) M. P. Aarnts, D. J. Stufkens, A. Oskam, J. Fraanje and K. Goubitz, *Inorganica Chimica Acta,* 1997, **256**, 93; (c) M. Shieh, Y. Y. Chu, M. H. Hsu, W. M. Ke and C. N. Lin, *Inorg. Chem.,* 2010, **50**, 565; (d) N. C. Burton, C. J. Cardin, D. J. Cardin, B. Twamley and Y. Zubavichus, *Organometallics,* 1995, **14**, 5708.

16 L. Yong, S. D. Hoffmann, T. F. Fässler, S. Riedel and M. Kaupp, *Angew. Chem. Int. Ed.,* 2005, **44**, 2092; *Angew. Chem.,* 2005, **117**, 2129.

17 (a) A. R. Kudinov, D. S. Perekalin, S. S. Rynin, K. A. Lyssenko, G. V. Grintselev-Knyazev and P. V. Petrovskii, *Angew. Chem. Int. Ed*., 2002, **41**, 4112; *Angew. Chem.,* 2002, **114**, 4286; (b) D. S. Perekalin, J. Holub, D. G. Golovanov, K. A. Lyssenko, P. V. Petrovskii, B. Štíbr and A. R. Kudinov, *Organometallics*, 2005, **24**, 4387.

18 (a) D. A. Roşca, K. Radkowski, L. M. Wolf, M. Wagh, R. Goddard, W. Thiel and A. Fürstner, *J. Am. Chem. Soc.,* 2017, **139**, 2443; (b) Y. Takahashi, Y. Nakajima, H. Suzuki and T. Takao, *Organometallics,* 2017, **36**, 3539; (c) K. Bakthavachalam, K. Yuvaraj, B. Mondal, R. Prakash and S. Ghosh, *Dalton. Trans*., 2015, **44**, 17920.

19 L. Pauling, *General Chemistry* 2nd ed.. W. H. Freeman. San Francisco. 1954.

20 S. Scharfe, T. F. Fässler, S. Stegmaier, S. D. Hoffmann and K. Ruhland, *Chem. Eur. J.,* 2008, **14**, 4479.

21 (a) X. Li, B. Kiran, J. Li, H.-J. Zh and L.-S. Wang, *Angew. Chem. Int. Ed.*, 2002, **41**, 4786; *Angew. Chem*., 2002, **114**, 4980; (b) P. Pyykkö and N. Runeberg, *Angew. Chem. Int. Ed.*, 2002, **41**, 2174; *Angew. Chem.*, 2002, **114**, 2278; (c) Y. Gao, S. Bulusu and X. C. Zeng, *J. Am. Chem. Soc.*, 2005, **127**, **45**, 15680.

22 H. B. Gray, Y. S. Sohn and N. Hendrickson, *J. Am. Chem. Soc.,* 1971, **93,** 3603.

23 (a) I. A. Popov, F.-X. Pan, X.-R. You, L.-J. Li, E. Matito, C. Liu, H.-J. Zhai, Z.-M. Sun, and A. I. Boldyrev, *Angew. Chem. Int. Ed.*, 2016, **55**, 15344; *Angew. Chem.* 2016, **128**, 15570; (b) X. Min, I. A. Popov, F.-X. Pan, L.-J. Li, E. Matito, Z.-M. Sun, L.-S. Wang, A. I. Boldyrev, *Angew. Chem. Int. Ed.*, 2016, **55**, 5531; *Angew. Chem.* 2016, **128**, 5621.

24 (a) A. Hirsch, Z. Chen and H. Jiao, *Angew. Chem. Int. Ed*., 2000, **39**, 3915; *Angew. Chem.,* 2000, **112**, 4079; (b) C. Liu, I. A. Popov, Z. Chen, A. I. Boldyrev and Z. -M. Sun, *Chem. Eur. J.,* 2018, **24**, 14583.

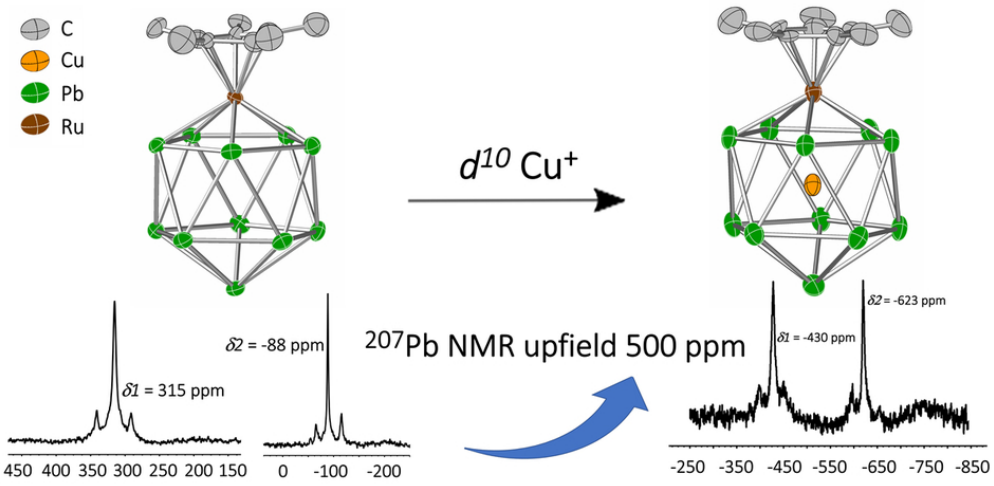

79x39mm (300 x 300 DPI)